Biophysical Reports

ARTICLE

A possible molecular mechanism for mechanotransduction at cellular focal adhesion complexes

Jichul Kim[1,*]
[1]Independent Researcher, Changwon, Republic of Korea

ABSTRACT Mechanotransduction at focal adhesion complexes is key for various cellular events. Theoretical analyses were performed to predict a potential role of lipid membranes in modulating mechanotransduction at focal adhesions. Calculations suggested that the size of nanostructural constraints and mechanical pulling applied on lipid membranes affect the generation of cellular traction forces and signaling transduction at focal adhesions. This work provides predictions on how lipid membranes contribute to mechanotransduction at cellular focal adhesions.

WHY IT MATTERS Focal adhesion machineries formed across cell membranes orchestrate a variety of signaling and adhesive molecules to function for important cellular physiologies. Although there are evidences that lipid membranes are involved in mechanical transduction at focal adhesions, how the detailed mechanical response of membranes contributes to the process is not identified yet. With many data previously identified, predictions made by theoretical modeling suggest that nonlinear pulling responses of lipid membranes serve as a key factor to interpret mechanotransduction at focal adhesions.

INTRODUCTION

Cells interact with their environments and generate traction forces through their adhesive molecular machinery formed across cell membranes. This collective molecular complex, called the focal adhesion (FA), orchestrates a variety of molecules such as adhesive integrin receptors inserted in membranes as well as talins and vinculins in cytoplasmic regions (1). Forces transmitted through these molecules generate biological signals that affect cellular growth, differentiation, migration, and tumor metastasis (2). Therefore, understanding FAs is central for various physiological and pathological processes.

Recent mechanical measurements identified the underlying molecular and biophysical mechanism of FAs from at the cellular level to the single-protein level. For example, the traction force microscopy technique enabled us to measure forces exserted by focal adhesion receptors with different extracellular rigidities (3,4). In addition, rheological methods (5), tension gauge tethers (6), and force sensors using fluorescence resonance energy transfer (FRET) technique (7) identified piconewton-scale mechanics important for the adhesion molecular machinery. Furthermore, single-molecule fluorescent imaging techniques provided information on the molecular length and count at FAs (8,9). More recently, the development of patterned nanolines unveiled how integrin receptors form nanoclusters at adhesion sites (10). Numerical investigations such as finite element simulations also provided predictions on cellular FAs (11,12). Despite the accumulated data and continued theoretical developments, an integrated interpretation on how individual molecular mechanism affects the generation of complex cellular mechanical behaviors and signaling transduction at FAs is still elusive. In addition, the mechanics of lipid membranes was investigated in numerous previous works on the adhesion machinery. For example, the mobility of adhesion receptors induced by forces on membranes was suggested as the physical basis for adhesion domain formation (13). Calculations were provided on membrane fluctuations at adhesion sites to predict properties on the nucleation of receptor-ligand domains (14,15). However, how the extension

Submitted May 26, 2021, and accepted for publication July 13, 2021.
*Correspondence: jichul0kim@gmail.com
Editor: Erdinc Sezgin.
https://doi.org/10.1016/j.bpr.2021.100006

versus force response of membranes contributes to mechanotransduction at FAs is not fully studied yet.

In this work, the combined nanomechanical responses of lipid membranes and talin proteins that incorporate vinculin molecules at FAs were calculated. How the nanoscale extension versus force response of the membrane-talin complex modulates opening, i.e., the activation, of cryptic vinculin binding sites (VBSs) in the talins was investigated. Furthermore, by connecting the membrane-talin response to other FA mechanisms, cellular traction forces on elastic substrates were calculated. Overall, this work provides an idea for the integrated FA molecular machinery by emphasizing a crucial role of lipid membranes in modulating mechanotransduction.

MATERIALS AND METHODS

Modeling the mechanical response of lipid membranes at the membrane-talin complex

Among various molecules, two components at FAs were mainly considered in this model: lipid membranes and talins (Fig. 1, *a* and *b*) (1). The lipid membrane was described as coarse-grained continuum by directly employing a finite element model introduced in a recent investigation (16). In this model, an energy functional for lipid membranes $\Psi_{membrane}$ was introduced as in Eq. 1.

$$\Psi_{membrane} = \int \left(2k_m H^2 + k_g K\right) dA + \int_{\alpha_0}^{\alpha_c} \sigma d\alpha \int dA. \quad (1)$$

The functional was expressed with energies associated with the mean H and Gaussian K curvatures of the surface of membranes (17,18). The mean curvature at a certain point of the surface can be $H = 0.5(h_{rr}/(\sqrt{1+h_r^{2}}^{3}) + h_r/(r\sqrt{1+h_r^{2}}))$, where h is the height function of the membrane shape and r is the rotational-symmetric radial function. The first and second derivatives of h with respect to r, h_r and h_{rr}, were expressed with respect to the parametric coordinate $s[0, 1]$ defined for the arclength of the membrane by using $h_r = h_s/r_s$ and $h_{rr} = h_{ss}/{r_s}^2 - h_s r_{ss}/{r_s}^3$, respectively (16). k_m and k_g are the bending modulus and the Gaussian curvature modulus, respectively. In performing variational calculations, the Gaussian curvature energy term in Eq. 1 was omitted, based on the Gauss-Bonnet theorem (19). For simplicity, k_m was assumed to be constant in this work (20–23). In Eq. 1, dA denotes the area element of the membrane.

The functional $\Psi_{membrane}$ contains another energy term for the area strain to consider the case in which lipid packing. i.e., the number of lipids per a smooth area, in the cell membrane is decreased with stretching. The strain energy density $\int_{\alpha_0}^{\alpha_c} \sigma d\alpha$ in Eq. 1 can be calculated by integrating the surface tension σ vs. area strain α relation from the resting reference strain α_0 to the strain under consideration α_c. Two smooth expressions for the surface tension are $\sigma = \sigma_0 \exp(8\pi k_m \alpha/(k_B T))$ for $\alpha \leq \alpha_{cross}$ and $\sigma = K_{app}(\alpha - \alpha_{cut})$ for $\alpha > \alpha_{cross}$, where α_{cut} and α_{cross} are the cutoff and crossover strains, respectively (16,24,25). K_{app} is the apparent area stretching modulus (16,24,25). The strain is $\alpha = (A^{res} - A_0^{res})/A_0^{res} = (\phi_0^{res} - \phi^{res})/\phi^{res}$, where A^{res} is the area of a lipid reservoir, A_0^{res} is the area of the reservoir at the resting reference configuration, ϕ^{res} is the uniform lipid number density, and ϕ_0^{res} is ϕ^{res} at the resting reference configuration. k_B is the Boltzmann constant, and T is temperature, where $k_B = 1.3806488 \times 10^{-23}$ J/K and $T = 300$ K in this work.

Boundary conditions are $(r(0), h(0)) = (r_{ca}, E_{mem\text{-}talin})$, $(r_s(0), h_s(0)) = (r_{ct} - r_{ca}, 0)$, $(r(1), h(1)) = (r_{ct}, 0)$, and $(r_s(1), h_s(1)) = (r_{ct} - r_{ca}, 0)$. $E_{mem\text{-}talin}$ is the shared extension of the membrane and the talin. r_{ca} defines the radius of a rigid area where clustered integrins are inserted (10,16). r_{ct} defines the radius of tented membranes in response to forces on the stiff cluster region (16). The membrane is clamped on the rigid cytoskeleton at the point apart from the center of the cluster by r_{ct}, whereas it is free to change curvatures within r_{ct}. Image data showing membrane curvatures at FAs may support this parameterization (26,27). Experiments evidenced that the mechanical extension of lipid membranes can be limited in living cells with

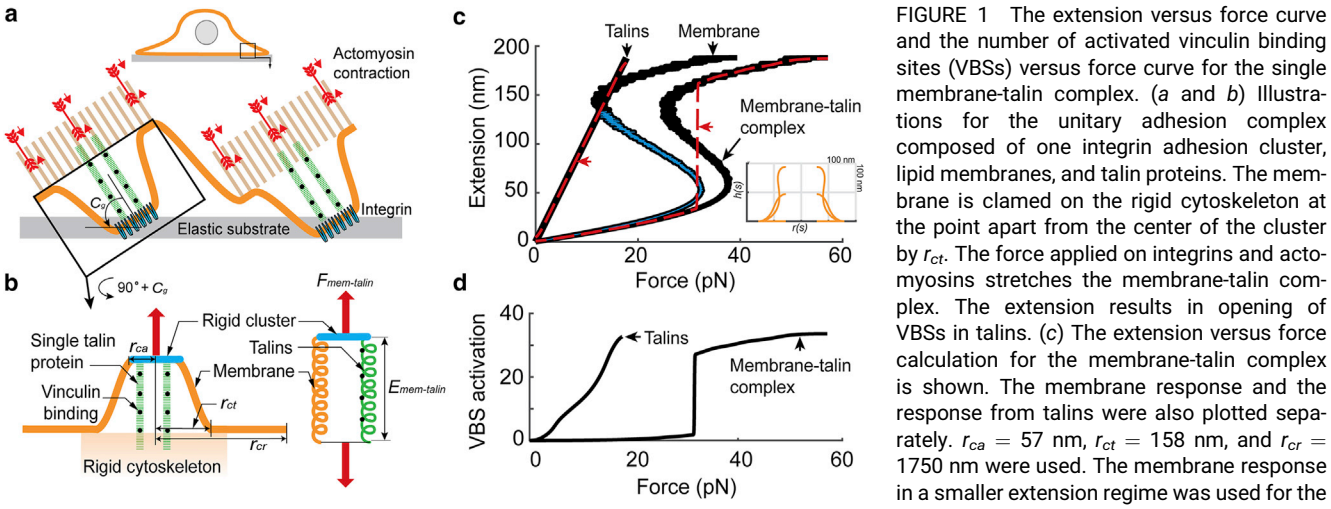

FIGURE 1 The extension versus force curve and the number of activated vinculin binding sites (VBSs) versus force curve for the single membrane-talin complex. (*a* and *b*) Illustrations for the unitary adhesion complex composed of one integrin adhesion cluster, lipid membranes, and talin proteins. The membrane is clamed on the rigid cytoskeleton at the point apart from the center of the cluster by r_{ct}. The force applied on integrins and actomyosins stretches the membrane-talin complex. The extension results in opening of VBSs in talins. (c) The extension versus force calculation for the membrane-talin complex is shown. The membrane response and the response from talins were also plotted separately. $r_{ca} = 57$ nm, $r_{ct} = 158$ nm, and $r_{cr} = 1750$ nm were used. The membrane response in a smaller extension regime was used for the calculation in Fig. 3 c, middle panel (*blue*). An inset demonstrates calculated shapes of the membrane component (the reservoir region was not plotted). Red arrows indicate the average extension versus force responses obtained by using the Boltzmann function. (*d*) The average number of activated VBSs versus force calculations for the membrane-talin complex and for the case without the mechanical rigidity of membranes (i.e., talins).

the increase of applied forces (16,28). These results suggested that the mobility of lipids in the cell membrane under mechanical deformation is allowed in a confined region. Therefore, the radius r_{cr} was introduced to assume the area of the lipid reservoir for the single membrane-talin complex. The size of the reservoir can be determined by $r_{cr} - r_{ct}$ and the domain $s[0, 1]$ (16). Here, the region defined by $r_{cr} - r_{ct}$ may not represent a physical geometry but simply determines the size of additional membrane materials that can undergo mechanical stretching (Fig. 1, *a* and *b*). In this work, $r_{cr} = 1750$ nm was mainly used.

Calculations for the membrane model were performed by using the finite element method provided in the previous work (16). In short, the functions $h(s)$ and $r(s)$ in the variational form of the energy functional were parameterized by using the B-spline function, and a system of nonlinear equations obtained from the variational formulation was solved by using the Newton-Raphson method (29). The stationary of Eq. 1 was assumed when the Euclidean norm of the difference between two subsequent solution vectors converged to a certain value. In increasing $E_{mem\text{-}talin}$, an estimate for the lipid number density for the $k + 1$st step was calculated from the kth step, when the calculated area of the tented membrane in the kth step is greater than that in the $k - 1$st step. Here, k is the index for step extensions. The evaluation of $h(s)$ and $r(s)$ functions and numerical integration were performed by using the Gaussian quadrature technique (30). See the previous work for details of the finite element model (16).

Modeling opening of VBSs in force-bearing talins at the membrane-talin complex

Talin molecules play pivotal roles for mechanical stabilities and transduction at FAs. They are linked to integrin adhesion clusters inserted in the membrane and interact with actin cytoskeletal structures directly or indirectly (7,10,31,32) (Fig. 1, *a* and *b*). Recent data measured by using elastic substrates whose stiffness can be variable and FRET tension sensors suggested that the average force applied on the single talin rod is ~4.5 pN in living cells (7). Therefore, the constant single talin force $F_{talin} = 4.5$ pN was used in this work. The total number of talin rods connected to one integrin cluster N_{talin} was calculated from $N_{talin} = C_{talin}N_{integrin}$. The number of integrin pairs $N_{integrin}$ in the area defined by r_{ca} can be $N_{integrin} = (r_{ca}/r_{integrin})^2$, where $r_{integrin}$ is the radius of the area occupied by one integrin pair (33,34). Experimental observations that demonstrated initial adhesion formation without talins (35); minimal and significant variations between the traction forces measured from normal and talin-depleted cells on soft and stiff substrates, respectively (4); and the substrate-rigidity-independent constant force applied on single talin rods (7) together suggested that the number of talins varies with the different level of mechanical stimuli applied on the single membrane-talin complex. Therefore, the number of talin molecules per one integrin pair C_{talin} was defined as a linear function of the membrane-talin extension in which $N_{talin} = 0$ and $N_{talin} = 3.92$ when $E_{mem\text{-}talin} = 0$ nm and $E_{mem\text{-}talin} = 187$ nm, respectively, for $r_{ca} = 57$ nm (Fig. S1). Here, about four talins interact with the single integrin cluster is consistent with the talin number measured from a nanoscale area of the living cell surface (9). Finally, the force applied on the single membrane-talin complex $F_{mem\text{-}talin}$ can be calculated from $F_{mem\text{-}talin} = F_{mem} + N_{talin}F_{talin}$ (Fig. 1 *b*).

Talin rods convert mechanical inputs into biological protein interactions. Opening of VBSs in force-bearing talins is one major event for mechanotransduction at FAs (36). A statistical description was introduced to predict the average number of activated VBSs with respect to the continuous application of forces to the membrane-talin complex. Previous experimental results from living cells demonstrated the gradient of the mechanical extension applied within the single talin rod, i.e., larger extensions near the head of the talin and smaller extensions near its tail region (7). This result suggested to assume sequential stretching of the talin rod from the head to the tail region with the continuous mechanical extension. The single talin rod has 11 cryptic VBSs (37). Therefore, by assuming a 4.5 nm unitary extension for 62 helices, the 11 extension values for opening of VBSs were defined as follows for the single talin rod: 18, 27, 40.5, 49.5, 54, 121.5, 148.5, 162, 207, 225, and 261 nm. Then, smooth N_{state} reference states can be obtained by interpolating discrete the number of activated VBSs versus extension data as shown in Fig. S2. With the 51 nm resting length of the talin (8,38) and the neck linker length up to 20 nm (37), the 332 nm total length when the 11 VBSs are opened by the constant force $F_{talin} = 4.5$ pN in this model is consistent with measured data obtained by using magnetic tweezers (5). By employing the Boltzmann function and assuming that the total energy of the membrane-talin complex for the ith state is $G_i^{tot} = G_i - F_{mem-talin}L_i^{ref}$, the probability of finding the ith state can be formulated as in Eq. 2 (39,40).

$$P_i = \frac{exp\left(-\beta G_i^{tot}\right)}{\sum_{j=1}^{N_{state}} exp\left(-\beta G_j^{tot}\right)} = \frac{1}{\sum_{j=1}^{N_{state}} exp\left[-\beta\left\{\left(G_j - G_i\right) - F_{mem-talin}\left(L_j^{ref} - L_i^{ref}\right)\right\}\right]}. \quad (2)$$

Here, G_i and L_i^{ref} are the internal energy and the reference extension for the ith state, respectively. G_i was calculated by integrating the force versus extension response of the membrane-talin complex (or the complex without the membrane rigidity) from the zero extension to L_i^{ref}. The constant β was obtained from $\beta = 1/(k_BT)$. From Eq. 2, the average number of activated VBSs $\overline{N}_{VBS}$ can be written as follows:

$$\overline{N}_{VBS} = \sum_{i=1}^{N_{state}} N_i^{VBS} P_i, \quad (3)$$

where N_i^{VBS} is the number of activated VBSs for the ith state (see Fig. S2, *orange curve*). Finally, the average number of activated VBSs at the single membrane-talin complex can be obtained by multiplying $\overline{N}_{VBS}$ and N_{talin}. Similarly, the average extension of the membrane-talin complex $\overline{E}_{mem-talin}$ can be calculated from Eq. 4.

$$\overline{E}_{mem-talin} = \sum_{i=1}^{N_{state}} L_i^{ref} P_i. \quad (4)$$

$N_{state} = 100$ was used to provide enough smoothness for the calculated Boltzmann's function curves.

Modeling cellular traction forces from the mechanical response of the membrane-talin complex

To investigate how the membrane-talin response contributes to the generation of cellular traction forces, the stiffness of extracellular substrates was modeled as in Eq. 5 by directly following previous investigations (Fig. 3, *a* and *b*) (3,4,41).

$$k_{substrate} = \frac{9F_{traction}r_a}{(4E_s)}. \quad (5)$$

Here, $k_{substrate}$ is the Young's modulus of substrates. $F_{traction}$ is the traction force to the substrate-horizontal direction applied on the area defined by the radius r_a. The normal component of the force was not considered in this work. $F_{traction}$ can be calculated from $F_{traction} = F_{mem\text{-}talin}N_{mem\text{-}talin}C_g/(\pi {r_a}^2)$, where $N_{mem\text{-}talin} = {r_a}^2/{r_{ct}}^2$ (or $N_{mem\text{-}talin} = 1$ when $r_a = r_{ca}$) is the number of the membrane-talin complex in the adhesion area. C_g is the geometric coefficient to account for the tilt of the molecular complex with respect to the substrates (see Fig. 3 *b*). It might be possible that the level of membrane-talin deformation affects the tilt angle of the complex. However, for simplicity, a constant C_g-value was used in this work. E_s is the lateral extension of substrates, and a condition $E_s = L_m - C_gE_{mem\text{-}talin} \geq 0$ should be satisfied. Here, L_m is the size of serial stretching of the substrate and the membrane-talin complex to the surface-horizontal direction. External mechanical stimuli such as shear stresses and intercellular mechanical interactions, as well as forces generated from the cellular interior region, can affect the mechanics at FAs (42,43). In this work, the contraction of actomyosins was assumed as the main force generating mechanism. Therefore, the L_m parameter is associated with the size of actomyosin contraction to the substrate-horizontal direction. Experimental data without external mechanical stimuli revealed that the inhibition of myosin II motor activities significantly reduced the magnitude of traction forces (4,44). Without full consideration on dynamic effects, this model assumed quasistatic configurations of FAs as similarly investigated in the experiment (4). All calculations and analyses were performed by using MATLAB (The MathWorks, Natick, MA). Parameter values used in this study are summarized in Fig. S3 and Table 1.

RESULTS

Nonlinear mechanical responses of lipid membranes modulate the activation of VBSs at the membrane-talin complex

The extension of the membrane-talin complex that resulted from changing forces is shown in Fig. 1 *c*. In this calculation, $r_{ca} = 57$ nm was used (10), where approximately four talin rods were connected in parallel with the membrane when the rigid cluster was displaced ~187 nm (9). $r_{ct} = 158$ nm and $r_{cr} = 1750$ nm were used (16). The response of the membrane-talin complex was nonlinear and showed negative extension-force slopes in an intermediate region, i.e., a snap-through instability. The negative stiffness was generated from the response of the membrane component. According to the previous research, the initial sharp curvature change and the accumulation of curvatures to prevent excessive stretching of the membrane area in the higher extension regime is responsible for the generation of this nonlinearity (16). In Fig. 1 *c*, how the Boltzmann function can generate the average extension versus force response was also evaluated for both the membrane-talin complex and the case without the membrane rigidity (Fig. 1 *c*, *red curves* indicated by *red arrows*). These curves provided comparisons between the characteristic extension values calculated from the analytic model and their thermodynamic average

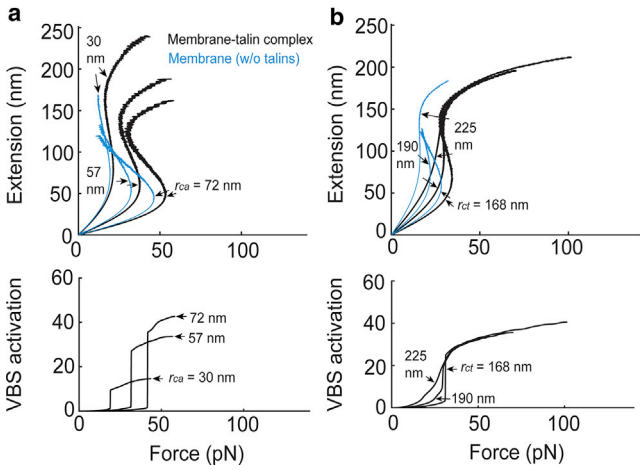

FIGURE 2 The modulation of the extension versus force curve and the number of activated VBSs versus force curve for the single membrane-talin complex. (*a*) Mechanical responses of the membrane-talin complex (*black*) and the complex without talin molecules (*blue*) by varying the r_{ca}-value. $r_{ct} = 158$ nm was used for all six calculations. Curves for the number of activated VBSs were plotted for the membrane-talin complex (*bottom panel*). (*b*) Responses with different r_{ct}-values. $r_{ca} = 57$ nm for all six calculations. See Fig. S5 for additional sensitivity analyses.

with respect to the applied force. A steep region was identified by using the Boltzmann function for the membrane-talin complex and that overlapped with the center of the negative stiffness region.

The average number of activated VBSs with the applied force was plotted in Fig. 1 *d*. When calculating the number of activated VBSs without considering the mechanical rigidity of lipid membranes, the value increased gradually in the force regime less than 20 pN (Fig. 1 *d*, talins). However, the curve was shifted to a higher force regime and transformed into the step-like form by considering the membrane connected in parallel with the talin rods (Fig. 1 *d*, membrane-talin complex). This result suggested that the deformation of membranes can modulate the activation of VBSs when the FA molecular machinery is mechanically stretched. The modulation of the VBS activation by the membrane demonstrated in Fig. 1, *c* and *d* was reminiscent of the mechanism of mechanical switches. Here, ~31.6 pN force in the steep region was similar to a previous measurement for the activation force of integrin signaling (6). The results in Fig. 1, *c* and *d* also demonstrated that the Boltzmann function widely used in interpreting biological signaling systems can be also used for mechanotransduction at FAs (47,48). Furthermore, the results support a notion that if a system shows signaling responses with two distinct states, there is a component that generates the snap-through instability (i.e., a mechanical bistability) (47).

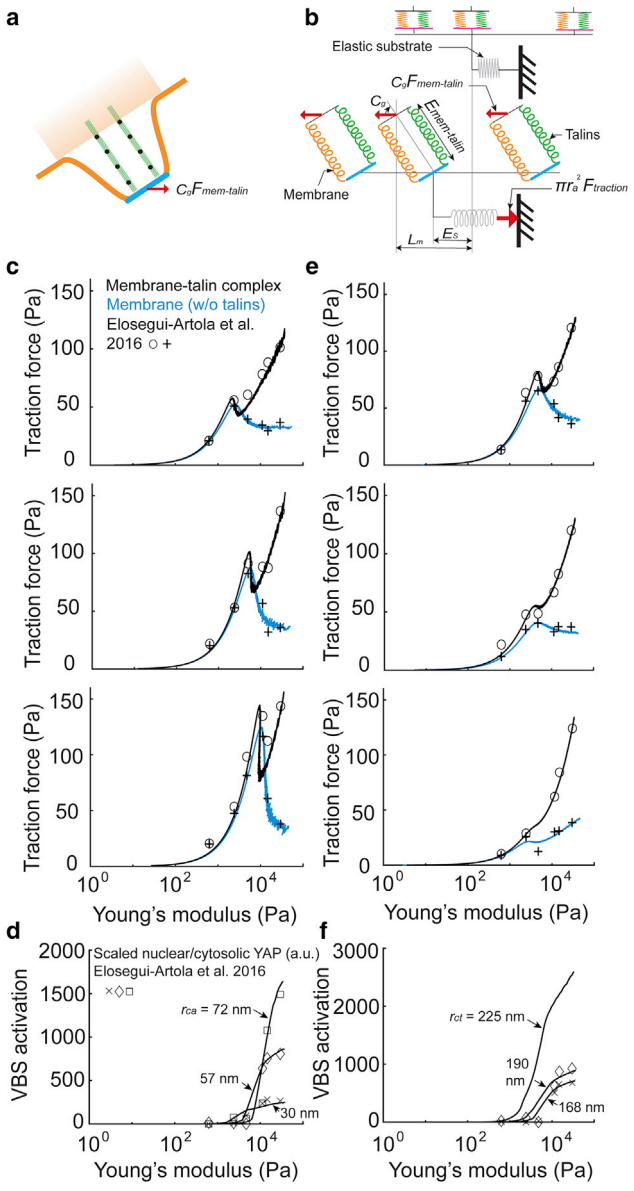

FIGURE 3 The cellular traction force versus substrate stiffness curves calculated from the responses of the membrane-talin complex. (*a* and *b*) Illustrations for how the single membrane-talin complex is linked to the generation of cellular traction forces at focal adhesions. (*c*) The traction forces calculated by using data in Fig. 2 *a*, top panel. $r_{ca} = 30$ nm (*top*), $r_{ca} = 57$ nm (*middle*), $r_{ca} = 72$ nm (*bottom*), and $r_{ct} = 158$ nm (*all*). The curves were compared to experimental measurements obtained by treating different amounts of fibronectin molecules on elastic substrates. (*d*) The number of activated VBSs in the area defined by r_a. The responses were calculated from the data in the bottom panel of Fig. 2 *a* by multiplying the number of activated VBSs per one membrane-talin complex and the number of membrane-talin complexes in the area defined by r_a. Measurements for fluorescent intensity ratios between YAPs located in the nucleus region and the cytosolic region were scaled and shown in the same plot. The fibronectin density was 1 μg/mL (*crosses*), 10 μg/mL (*diamonds*), or 100 μg/mL (*squares*) in the experiments. (e) The traction forces calculated by using the data in the top panel of Fig. 2 *b*. $r_{ct} = 168$ nm (*top*), $r_{ct} = 190$ nm (*middle*), $r_{ct} = 225$ nm (*bottom*), and $r_{ca} = 57$ nm (*all*). The curves were compared to measurements obtained by treating different amounts of the integrin-binding peptide GPen. (*f*) The number of activated VBSs in the area defined by r_a. The responses were calculated from the data in the bottom panel of Fig. 2 *b*. Scaled fluorescent intensity ratios between YAPs in the nucleus region and the cytosolic region (with GPen) are also shown. The GPen concentration was 0.05 mM (*crosses*) and 0.15 mM (*diamonds*) in the experiments. All measured data were obtained from (4).

The size of nanostructural constraints applied on lipid membranes modulates the activation of VBSs at the membrane-talin complex

The idea that pulling of cell surface receptors can generate nonlinear nanomechanical responses was recently evidenced experimentally (16). Analyses suggested that the responses can be modulated by the interaction of bilayers with rigid components (16). Therefore, the size of the adhesion cluster and the level of the membrane-cytoskeleton interaction can serve important roles in modulating the mechanical response and the VBS activation at FAs. To test these possibilities, the r_{ca}- and r_{ct}-values were systematically varied in calculating the extension versus force curve and the activation of VBSs versus force curve for the membrane-talin complex. As shown with black curves in Fig. 2 *a*, increasing r_{ca} resulted in responses that showed more predominant sigmoidal nonlinearity. An initial force peak in the response, i.e., a signature for the generation of the negative stiffness, was shifted to a higher force regime by increasing r_{ca}. Shifting of the curve for the VBS activation was also identified, and the force peak of each extension versus force curve approximately overlapped with the steep region of the VBS activation curve. As shown in Fig. 2 *b*, the shapes of the extension versus force curve and the VBS activation versus force curve were also changed by varying r_{ct} from 168 to 190 nm and 225 nm. However, the shifting characteristic shown in Fig. 2 *a* was not significant here. Instead, curves in Fig. 2 *b* demonstrated that the sharpness of the step-like behavior in the activation curve was reduced when the r_{ct}-value was increased. In Fig. 2, the responses of the unit complex without the talin molecules connected to the integrin cluster were also plotted (*blue curves*). Deformed shapes for the membrane component are supplemented in Fig. S4. Additional sensitivity analyses for r_{ca} and r_{ct} are shown in Fig. S5. A sensitivity study for r_{ct} and r_{cr} is shown in Fig. S6.

The nonlinear mechanical responses and the nanostructural constraints on the membrane-talin complex affect the generation of cellular traction forces at FAs

By using the responses shown in Fig. 1 c, traction force versus substrate stiffness responses were generated

TABLE 1 The summary of parameter values

Parameters	Used values
k_m (lipid bilayer bending modulus) (24)	32 k_BT[a,b]
σ_0 (lipid bilayer surface tension with the zero strain, i.e., $\alpha = 0$) (16)	exp(−10) mN/m[a,b]
K_{app} (lipid bilayer apparent area stretching modulus) (24)	275 mN/m[a,b]
r_{ca} (radius of integrin clusters) (10)	30, 57, 72 nm[c]
r_{ct} (radius of tented membranes)	158, 168, 190, 225 nm[c,d]
r_{cr} (radius of lipid reservoirs)	1750 nm[d,e]
$r_{integrin}$ (radius of the area occupied by one integrin pair) (33,34)	5 nm
F_{talin} (constant force applied on single talins) (7)	4.5 pN
C_g (geometric tilt coefficient)	0.21[f]
L_m (size of actomyosin contraction to the substrate lateral direction)	3.74–60.74 nm[c]
r_a (radius of the adhesion area)	57–1800 nm[c]

[a]Sensitivity studies for k_m, σ_0, and K_{app} on the extension versus force response of the membrane are supplemented in Fig. S10.
[b]With $r_{ca} = 57$ nm, $r_{ct} = 158$ nm, and $r_{cr} = 1750$ nm, the surface tension σ of the membrane at $E_{mem\text{-}talin} = 188$ nm was ~0.0612 mN/m (45).
[c]See Fig. S3 for how these parameters were varied.
[d]These are similar with the r_{ct}- and r_{cr}-values estimated from the upper surface of living cells (16).
[e]A sensitivity study for r_{cr} is supplemented in Fig. S6.
[f]This value assumed for the average tilt of the membrane-talin complex on continuous elastic substrates is smaller than the value measured from elastic tethers linked to integrins and a rigid substrate by a factor of 3 (46).

in Fig. 3 *c*, middle panel. The traction force responses with and without talins also showed nonlinear mechanical characteristics. The functionality of talin rods is closely related to the number of integrin clusters and myosin II activities at FAs (35,49). Therefore, r_a and L_m were differently assigned for the traction force calculation for the membrane-talin complex and the membrane without talins connected to integrin clusters (Fig. S3). It was remarkable that direct comparisons between the calculations and previously measured data from living cells showed good agreement for both the membrane-talin and membrane-without-talin components (4) (Fig. 3 *c*, *middle panel*). As a note, nontrivial mismatches were invoked in the comparison when using same r_a- and L_m-values (see Fig. S7). Similarly, as shown in Fig. 1, *c* and *d*, the negative slope region of the force versus stiffness response (Fig. 3 *c*, *middle panel*, *black*) overlapped with the steep region of the curve for the VBS activation (Fig. 3 *d*, $r_{ca} = 57$ nm). It is well known that the localization of yes-associated proteins (YAPs), the transcriptional regulators within cells, serves as an important indicator for mechanotransduction associated with FAs (4). Therefore, a comparison between the calculation for the VBS activation at the membrane-talin complex and measurements for the nucleus/cytosolic ratio of YAPs was provided in Fig. 3 *d* ($r_{ca} = 57$ nm and *diamonds*). There was an agreement for the onset of the VBS activation and the YAP localization to the nucleus region. The comparison demonstrated the membrane-talin complex as an important component in modulating mechanotransduction associated with FAs.

The effect of r_{ca} on cellular traction forces was investigated. For this purpose, the membrane-talin and membrane-without-talin calculations using $r_{ca} = 30$ nm and $r_{ca} = 72$ nm shown in Fig. 2 *a* were further analyzed to plot the traction force versus substrate stiffness responses in Fig. 3 *c*, top and bottom, respectively. Here, the r_a-value was increased with r_{ca} based on a recent identification that the increase of the size of integrin clusters is positively correlated with that of the FA area (10). In addition, the L_m-value was decreased because the increase of r_{ca} results in stiffer membrane-talin complexes (see Fig. S3). Gradual changes in the traction force responses were identified by increasing r_{ca}. These changes in the traction forces showed good agreements with living cell measurements obtained by varying the density of fibronectin molecules treated on the surface of substrates (4) (Fig. 3 *c*). The result suggested a tendency that the increase of the fibronectin density can result in the increase of the integrin cluster size. In Fig. S8, the r_{ca} vs. fibronectin density relation was plotted. Shifting of the VBS activation curve to a high stiffness regime was identified in increasing r_{ca} (Fig. 3 *d*). Comparisons between the onsets of the VBS activation with different r_{ca}-values and the localization of YAPs to the nucleus region with different fibronectin densities showed good agreements.

Investigating how r_{ct} affects the generation of traction forces provided a membrane-based hypothesis for a widely recognized pharmacological method using peptide sequences to modulate the integrin-ligand interaction (50–52). According to the previous investigation, the treatment of the peptide called GPen to inhibit $\alpha_v\beta_3$ without affecting $\alpha_5\beta_1$ integrins reduces the nonlinearity in the force versus stiffness response generated from talin-1-null but talin-2-sufficient cells (4). To reduce the nonlinearity in this model framework, either r_{ca} is decreased or r_{ct} is increased. It was reported that the peptide treatment results in a talin-depleted phenotype (52), and another reported that the dysfunction of talins does not affect the size of adhesion clusters (49). These suggested the investigation of a relation between the effect of the peptide treatment in living cells and the effect of changing r_{ct}, not r_{ca}, in the mechanical response of the membrane-talin model.

To compare the calculations in Fig. 2 *b* to traction force versus substrate stiffness measurements from the peptide-treated cells (4), the r_a- and L_m-values were systematically increased with the increase of r_{ct}

(Fig. S3). Direct comparisons between the calculations and the measurements showed good agreements (Fig. 3 *e*). The result suggested that the integrin-binding peptide can modulate the size of the tented lipid membrane without directly affecting the size of integrin clusters. The relation between r_{ct} and the peptide concentration is shown in Fig. S8. The curves for the VBS activation were plotted in Fig. 3 *f* and compared to the measurements for the YAP localization. Overall, it might be important to investigate whether and how the complex of $\alpha_5\beta_1$ integrins and talin-2 molecules is stretched and slides on lipid membranes to contribute to modulating r_{ct} when the FA is mechanically perturbed (53).

DISCUSSION

The generation of mechanical forces and signaling transduction at FAs are key for various cellular physiologies. Several theoretical models were proposed to explain observed mechanical responses at FAs, based on dynamic binding between different molecular components (3,4,54) as well as the unfolding property of adaptor proteins (4). In this work, another possibility is proposed by asking how the lipid membrane mechanics contributes to mechanotransduction at FAs. Combined extension versus force responses of membranes and talins were nonlinear. According to sensitivity analyses, this nonlinearity can be modified by changing the size of nanostructural constraints applied on the lipid membrane component, and that was linked to the opening of VBSs in talin rods. The results suggested that the membrane pulling mechanics determined by r_{ca} and r_{ct} serves as an important factor to modulate mechanotransduction at FAs. This work also suggested the modulation of r_{ca}, r_{ct}, and r_{cr} as a potent target for nanomechanical and biochemical drug developments for tuning the two-state shape and the shifting characteristic of signaling transduction responses. In the same line, the identification of molecular and genetic components responsible for achieving the optimal size of r_{ca}, r_{ct}, and r_{cr} would be important.

Cells are complex and involved in many active mechanisms related to each other. Therefore, the simple membrane parameters were insufficient, and the model required several other parameters, i.e., C_g, L_m, and r_a, to translate the membrane-talin responses into the cellular traction forces (see Fig. S3 and Table 1 for how the parameters were varied). To demonstrate the importance of these parameters at FAs, analyses performed by varying L_m and r_a with fixed membrane parameters were supplemented in Fig. S9 and compared with measurements. It might be possible that other nanomechanical characteristics of membranes generated by the effect of multiple r_{cr} (16) and osmosis (6) are also important for the mechanism of FAs. In addition, lipid composition that directly affects the mechanical moduli of membranes can influence the mechanical response at FAs (55,56) (see Fig. S10).

The model directly employed and regenerated key experimental data measured at FAs. These include the size of single integrin clusters (10), the integrin activation force (6), the number of talin proteins within a nanoscale area (9), and the traction force versus substrate stiffness responses of living cells (4) (also see Table 1). It was remarkable that by simply assuming pulling of lipid membranes at FAs, those measured data mutually supported their validity. Similar membrane analyses performed for another mechanosensitive system may provide additional support for this work by suggesting that the nanomechanical response of lipid membranes is commonly important for signaling systems mediated by adhesion receptors (57). Overall, with an emphasis on the mechanics of lipid membranes, this work provides an integrated molecular mechanism for the generation of cellular traction forces and signaling transduction at FAs.

SUPPORTING MATERIAL

Supplemental information can be found online at https://doi.org/10.1016/j.bpr.2021.100006.

DECLARATION OF INTERESTS

The author declares no competing interests.

REFERENCES

1. Kanchanawong, P., G. Shtengel, …, C. M. Waterman. 2010. Nanoscale architecture of integrin-based cell adhesions. *Nature.* 468:580–584.
2. Sun, Z., S. S. Guo, and R. Fässler. 2016. Integrin-mediated mechanotransduction. *J. Cell Biol.* 215:445–456.
3. Elosegui-Artola, A., E. Bazellières, …, P. Roca-Cusachs. 2014. Rigidity sensing and adaptation through regulation of integrin types. *Nat. Mater.* 13:631–637.
4. Elosegui-Artola, A., R. Oria, …, P. Roca-Cusachs. 2016. Mechanical regulation of a molecular clutch defines force transmission and transduction in response to matrix rigidity. *Nat. Cell Biol.* 18:540–548.
5. Yao, M., B. T. Goult, …, J. Yan. 2016. The mechanical response of talin. *Nat. Commun.* 7:11966.
6. Wang, X., and T. Ha. 2013. Defining single molecular forces required to activate integrin and notch signaling. *Science.* 340:991–994.
7. Ringer, P., A. Weißl, …, C. Grashoff. 2017. Multiplexing molecular tension sensors reveals piconewton force gradient across talin-1. *Nat. Methods.* 14:1090–1096.
8. Margadant, F., L. L. Chew, …, M. Sheetz. 2011. Mechanotransduction in vivo by repeated talin stretch-relaxation events depends upon vinculin. *PLoS Biol.* 9:e1001223.

9. Fischer, L. S., C. Klingner, …, C. Grashoff. 2021. Quantitative single-protein imaging reveals molecular complex formation of integrin, talin, and kindlin during cell adhesion. *Nat. Commun.* 12:919.
10. Changede, R., H. Cai, …, M. P. Sheetz. 2019. Integrin nanoclusters can bridge thin matrix fibres to form cell-matrix adhesions. *Nat. Mater.* 18:1366–1375.
11. Mullen, C. A., T. J. Vaughan, …, L. M. McNamara. 2014. Cell morphology and focal adhesion location alters internal cell stress. *J. R. Soc. Interface.* 11:20140885.
12. Rens, E. G., and R. M. H. Merks. 2020. Cell shape and durotaxis explained from cell-extracellular matrix forces and focal adhesion dynamics. *iScience.* 23:101488.
13. Smith, A.-S., K. Sengupta, …, E. Sackmann. 2008. Force-induced growth of adhesion domains is controlled by receptor mobility. *Proc. Natl. Acad. Sci. USA.* 105:6906–6911.
14. Bihr, T., U. Seifert, and A.-S. Smith. 2012. Nucleation of ligand-receptor domains in membrane adhesion. *Phys. Rev. Lett.* 109:258101.
15. Bihr, T., S. Fenz, …, A.-S. Smith. 2014. Association rates of membrane-coupled cell adhesion molecules. *Biophys. J.* 107:L33–L36.
16. Kim, J. 2020. Probing nanomechanical responses of cell membranes. *Sci. Rep.* 10:2301.
17. Canham, P. B. 1970. The minimum energy of bending as a possible explanation of the biconcave shape of the human red blood cell. *J. Theor. Biol.* 26:61–81.
18. Helfrich, W. 1973. Elastic properties of lipid bilayers: theory and possible experiments. *Z. Naturforsch. C.* 28:693–703.
19. Powers, T. R., G. Huber, and R. E. Goldstein. 2002. Fluid-membrane tethers: minimal surfaces and elastic boundary layers. *Phys. Rev. E Stat. Nonlin. Soft Matter Phys.* 65:041901.
20. Helfrich, W. 1985. Effect of thermal undulations on the rigidity of fluid membranes and interfaces. *J. Phys. (Paris).* 46:1263–1268.
21. Peliti, L., and S. Leibler. 1985. Effects of thermal fluctuations on systems with small surface tension. *Phys. Rev. Lett.* 54:1690–1693.
22. Kleinert, H. 1986. Thermal softening of curvature elasticity in membranes. *Phys. Lett. A.* 114:263–268.
23. Deserno, M. 2005. The influence of thermal fluctuations on the bending rigidity of fluid membranes.
24. Evans, E., and W. Rawicz. 1990. Entropy-driven tension and bending elasticity in condensed-fluid membranes. *Phys. Rev. Lett.* 64:2094–2097.
25. Rawicz, W., K. C. Olbrich, …, E. Evans. 2000. Effect of chain length and unsaturation on elasticity of lipid bilayers. *Biophys. J.* 79:328–339.
26. Medalia, O., and B. Geiger. 2010. Frontiers of microscopy-based research into cell-matrix adhesions. *Curr. Opin. Cell Biol.* 22:659–668.
27. Paszek, M. J., C. C. DuFort, …, V. M. Weaver. 2014. The cancer glycocalyx mechanically primes integrin-mediated growth and survival. *Nature.* 511:319–325.
28. Raucher, D., and M. P. Sheetz. 1999. Characteristics of a membrane reservoir buffering membrane tension. *Biophys. J.* 77:1992–2002.
29. Ben-Israel, A. 1966. A Newton-Raphson method for the solution of systems of equations. *J. Math. Anal. Appl.* 15:243–252.
30. Abramowitz, M., and I. A. Stegun. 1972. Handbook of Mathematical Functions: With Formulas, Graphs, and Mathematical Table. National Bureau of Standards, Washington, DC.
31. Calderwood, D. A., R. Zent, …, M. H. Ginsberg. 1999. The Talin head domain binds to integrin β subunit cytoplasmic tails and regulates integrin activation. *J. Biol. Chem.* 274:28071–28074.
32. Srivastava, J., G. Barreiro, …, D. L. Barber. 2008. Structural model and functional significance of pH-dependent talin-actin binding for focal adhesion remodeling. *Proc. Natl. Acad. Sci. USA.* 105:14436–14441.
33. Gjelstrup, L. C., T. Boesen, …, T. Vorup-Jensen. 2010. Shedding of large functionally active CD11/CD18 integrin complexes from leukocyte membranes during synovial inflammation distinguishes three types of arthritis through differential epitope exposure. *J. Immunol.* 185:4154–4168.
34. Xu, X.-P., E. Kim, …, D. Hanein. 2016. Three-dimensional structures of full-length, membrane-embedded human α(IIb)β(3) integrin complexes. *Biophys. J.* 110:798–809.
35. Zhang, X., G. Jiang, …, M. P. Sheetz. 2008. Talin depletion reveals independence of initial cell spreading from integrin activation and traction. *Nat. Cell Biol.* 10:1062–1068.
36. del Rio, A., R. Perez-Jimenez, …, M. P. Sheetz. 2009. Stretching single talin rod molecules activates vinculin binding. *Science.* 323:638–641.
37. Goult, B. T., X.-P. Xu, …, D. Hanein. 2013. Structural studies on full-length talin1 reveal a compact auto-inhibited dimer: implications for talin activation. *J. Struct. Biol.* 184:21–32.
38. Goldmann, W. H., A. Bremer, …, G. Isenberg. 1994. Native talin is a dumbbell-shaped homodimer when it interacts with actin. *J. Struct. Biol.* 112:3–10.
39. Ursell, T., J. Kondev, …, R. RobPhillips. 2008. Role of lipid bilayer mechanics in mechanosensation. *In* Mechanosensitive Ion Channels. A. Kamkin and I. Kiseleva, eds. Springer, pp. 37–70.
40. Sevcik, C. 2017. Caveat on the Boltzmann distribution function use in biology. *Prog. Biophys. Mol. Biol.* 127:33–42.
41. Ghibaudo, M., A. Saez, …, B. Ladoux. 2008. Traction forces and rigidity sensing regulate cell functions. *Soft Matter.* 4:1836–1843.
42. Muhamed, I., J. Wu, …, D. E. Leckband. 2016. E-cadherin-mediated force transduction signals regulate global cell mechanics. *J. Cell Sci.* 129:1843–1854.
43. Vining, K. H., and D. J. Mooney. 2017. Mechanical forces direct stem cell behaviour in development and regeneration. *Nat. Rev. Mol. Cell Biol.* 18:728–742.
44. Kovács, M., J. Tóth, …, J. R. Sellers. 2004. Mechanism of blebbistatin inhibition of myosin II. *J. Biol. Chem.* 279:35557–35563.
45. Morris, C. E., and U. Homann. 2001. Cell surface area regulation and membrane tension. *J. Membr. Biol.* 179:79–102.
46. Brockman, J. M., A. T. Blanchard, …, K. Salaita. 2018. Mapping the 3D orientation of piconewton integrin traction forces. *Nat. Methods.* 15:115–118.
47. Howard, J., and A. J. Hudspeth. 1988. Compliance of the hair bundle associated with gating of mechanoelectrical transduction channels in the bullfrog's saccular hair cell. *Neuron.* 1:189–199.
48. Häse, C. C., A. C. Le Dain, and B. Martinac. 1995. Purification and functional reconstitution of the recombinant large mechanosensitive ion channel (MscL) of *Escherichia coli*. *J. Biol. Chem.* 270:18329–18334.
49. Changede, R., X. Xu, …, M. P. Sheetz. 2015. Nascent integrin adhesions form on all matrix rigidities after integrin activation. *Dev. Cell.* 35:614–621.
50. Pierschbacher, M. D., and E. Ruoslahti. 1987. Influence of stereochemistry of the sequence Arg-Gly-Asp-Xaa on binding specificity in cell adhesion. *J. Biol. Chem.* 262:17294–17298.
51. Ruoslahti, E. 1996. RGD and other recognition sequences for integrins. *Annu. Rev. Cell Dev. Biol.* 12:697–715.
52. Roca-Cusachs, P., N. C. Gauthier, …, M. P. Sheetz. 2009. Clustering of α(5)β(1) integrins determines adhesion strength whereas α(v)β(3) and talin enable mechanotransduction. *Proc. Natl. Acad. Sci. USA.* 106:16245–16250.
53. Yuan, Y., L. Li, …, C. Huang. 2017. The molecular basis of talin2's high affinity toward β1-integrin. *Sci. Rep.* 7:41989.

54. Chan, C. E., and D. J. Odde. 2008. Traction dynamics of filopodia on compliant substrates. *Science.* 322:1687–1691.

55. Sharma, D. K., J. C. Brown, …, R. E. Pagano. 2005. The glycosphingolipid, lactosylceramide, regulates β1-integrin clustering and endocytosis. *Cancer Res.* 65:8233–8241.

56. Takechi-Haraya, Y., K. Sakai-Kato, …, Y. Goda. 2016. Atomic force microscopic analysis of the effect of lipid composition on liposome membrane rigidity. *Langmuir.* 32:6074–6082.

57. Kim, J. 2015. Unconventional mechanics of lipid membranes: a potential role for mechanotransduction of hair cell stereocilia. *Biophys. J.* 108:610–621.